www.nature.com/aps

Acta Pharmacologica Sinica

ARTICLE

# Itraconazole and rifampicin, as CYP3A modulators but not P-gp modulators, affect the pharmacokinetics of almonertinib and active metabolite HAS-719 in healthy volunteers

Lu Liu[1,2], Wei Li[1], Le Yang[1,2], Zi-tao Guo[1], Hao Xue[1], Ning-jie Xie[1,2] and Xiao-yan Chen[1,2]

Almonertinib is a novel third-generation EGFR tyrosine kinase inhibitor. It is mainly metabolized by CYP3A in vitro, and *N*-desmethylated almonertinib (HAS-719) is the major active metabolite in human plasma. In this study, we investigated the effects of CYP3A inhibitor itraconazole and CYP3A inducer rifampicin on the pharmacokinetics of almonertinib and HAS-719 in 64 healthy volunteers. We found that when co-administered with itraconazole, the maximal plasma concentration ($C_{max}$) and the plasma exposure ($AUC_{0-t}$) of almonertinib were increased by 56.3% and 2.38-fold, respectively, whereas the $C_{max}$ and $AUC_{0-t}$ of HAS-719 were reduced by 86.8% and 71.8%, respectively. Co-administration with rifampicin reduced the $C_{max}$ and $AUC_{0-t}$ of almonertinib by 79.3% and 92.6%, but the $AUC_{0-t}$ of HAS-719 was unexpectedly decreased by 72.5%. In vitro assays showed that both almonertinib and HAS-719 were substrates of CYP3A and P-gp. Co-administration of rifampicin in Beagle dogs reduced the fecal recovery of almonertinib and HAS-719, and markedly increased the levels of metabolites derived from further metabolism of HAS-719, which was consistent with human plasma data, suggesting that although rifampicin was also a potent inducer of P-gp, the pharmacokinetic alternation of HAS-719 was mainly due to its further metabolism but not excretion changes. Moreover, we revealed that almonertinib was a moderately sensitive substrate of CYP3A in vivo. Special attention should be paid to the interaction between almonertinib and drugs or food affecting CYP3A activity in the clinical application of almonertinib.

**Keywords:** almonertinib; itraconazole; rifampicin; drug metabolism; drug interaction; CYP3A; P-gp; pharmacokinetics

*Acta Pharmacologica Sinica* (2022) 43:1082–1090; https://doi.org/10.1038/s41401-021-00710-8

## INTRODUCTION

Epidermal growth factor receptor (EGFR) is a transmembrane protein with cytoplasmic kinase activity, which transduces growth factor signaling from the extracellular milieu to the cell. In pathological settings, the EGFR is a driver of tumorigenesis in lung and breast cancer, and glioblastoma. Inappropriate activation of the EGFR mainly results from amplification and point mutations at the genomic locus [1]. Cancers with EGFR mutations are often sensitive to treatment with EGFR tyrosine kinase inhibitors (TKIs) [2], which can inhibit the activity and intracellular phosphorylation of EGFR-related tyrosine kinase and block EGFR-induced tumor cell growth by competitively binding to adenine nucleoside triphosphate sites on the intracellular tyrosine kinase domain, thereby inhibiting tumor metastasis [3].

Tumors with EGFR mutations account for approximately 10%–40% of non-small cell lung cancer (NSCLC) worldwide [4]. Despite initial beneficial response to first generation EGFR-TKIs, including gefitinib and erlotinib, the majority of patients will develop disease progression within 1 to 2 years due to acquired resistance [5, 6]. The most frequently reported mechanism of acquired resistance is the EGFR T790M point mutation within an exon, and this has been detected in >50% of NSCLC patients [7, 8]. The second-generation of EGFR-TKIs such as afatinib and dacomitinib have not overcome T790M resistance because of adverse side effects [9].

Almonertinib (HS-10296, N-(5-((4-(1-cyclopropyl-1H-indol-3-yl) pyrimidin-2-yl) amino)-2-((2-(dimethylamino) ethyl) (methyl) amino)-4-methoxyphenyl) acrylamide, Fig. 1a) is a novel third-generation EGFR TKI. It is a potent and highly selective wild type and mutant EGFR irreversible inhibitor that has been approved for the treatment of NSCLC patients with EGFR mutations [10, 11]. In vitro enzymology and cell proliferation studies displayed that almonertinib has a strong inhibitory effect on EGFR T790M mutations but a weaker inhibitory effect on wild-type EGFR. *N*-Desmethylated almonertinib (HAS-719) (Fig. 1b) has been identified as a main metabolite of almonertinib in human plasma. Incubation with recombinant CYP enzymes or human liver microsomes indicates that CYP3A is primarily responsible for the metabolic clearance of almonertinib (Supplementary Fig S1 and Table S1).

Almonertinib may be used in combination with other drugs in clinical treatment, which may include inhibitors or inducers of CYP3A. This may lead to drug–drug interactions with serious adverse effects or reduced efficacy. The main purpose of this study was to evaluate the effects of oral administration of a strong CYP3A inhibitor (itraconazole) or inducer (rifampicin) on the pharmacokinetic (PK) profile of almonertinib and its active

[1]Shanghai Institute of Materia Medica, Chinese Academy of Sciences, Shanghai 201203, China and [2]University of Chinese Academy of Sciences, Beijing 100049, China
Correspondence: Xiao-yan Chen (xychen@simm.ac.cn)

Received: 4 February 2021 Accepted: 30 May 2021
Published online: 15 July 2021

metabolite HAS-719 in healthy subjects to determine relationship between dose, exposure and effect.

## MATERIALS AND METHODS

### Chemicals

Almonertinib tablets were manufactured by Jiangsu Hansoh Pharmaceutical Group Co. Ltd. (Lianyungang, China). Rifampicin capsules were purchased from SANOFI AVENTIS US LLC (Paris, France) and itraconazole capsules were supplied by Xi-an Janssen Pharmaceutical Co., Ltd. (Xi-an, China). Reference standards of almonertinib (purity 99.3%) and HAS-719 (purity 99.6%) were provided kindly by Jiangsu Hansoh Pharmaceutical Group Co. Ltd. (Lianyungang, China). The internal standard d6-HAS-000719 was provided by Shanghai Hansoh Biomedical Co. Ltd. (Shanghai, China). GF120918, digoxin (P-gp-positive substrate), DMEM medium, fetal bovine serum (FBS), *L*-glutamine, nonessential amino acids, 0.25% trypsin, penicillin G and streptomycin were purchased from Invitrogen (Carlsbad, CA, USA). Pooled human liver microsomes and recombinant CYP enzymes, including CYP1A2, 2A6, 2B6, 2C8, 2C9, 2C19, 2D6, 2E1, 3A4, and 3A5 were purchased from BD Gentest (Woburn, MA, USA). Nicotinamide adenine dinucleotide phosphate (NADPH), ketoconazole and 1-aminobenzotriazole were purchased from Sigma-Aldrich (St. Louis, MO, USA). Madin-Darby canine kidney cells (MDCKII)-MDR1 (multidrug resistance protein 1/P-gp transfected cells) were kindly provided by Prof Hong-jian Zhang from the School of Pharmacy, Soochow University (Suzhou, China).

### Clinical studies

*Ethics*. The research protocol and informed consent documents were reviewed and approved by the Ji-nan Central Hospital Ethics Committee (Ji-nan, China). According to the 1964 Helsinki Declaration, the design and monitoring of clinical studies were consistent with the ethical principles of good clinical practice. Each eligible study subject was required to read and sign a consent form prior to study entry.

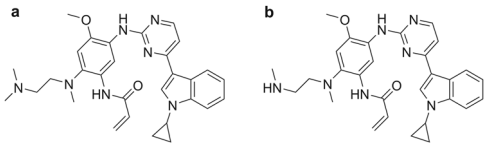


**Fig. 1** Structure of almonertinib (**a**) and HAS-719 (**b**).

*Study design*. A total of 64 subjects were randomized into two study arms to evaluate the effects of co-administration of itraconazole (study 1) or rifampicin (study 2) on almonertinib PK. Key inclusion and exclusion criteria for the studies are provided in Table 1. Both study 1 and study 2 were open-label, double-cycle, single-sequence, crossover clinical studies and included two treatment periods separated by a wash-out period of 21 days.

In study 1, subjects received a single 110 mg oral dose of almonertinib on day 1. Then subjects received itraconazole 200 mg twice daily for 12 days (days 19–30). On the morning of day 22, subjects received itraconazole 400 mg together with a single 110-mg dose of almonertinib.

In study 2, subjects received a single 110 mg oral dose of almonertinib on day 1. Then subjects received rifampicin 600 mg once daily for 15 days (days 16–30), and on the morning of day 22, they received rifampicin 600 mg together with a single 110-mg dose of almonertinib.

*Sample collection and analysis*. For determination of almonertinib and HAS-719 levels in plasma, venous blood samples (4 mL) were collected in tubes containing ehylene diamine tetraacetic acid-2K (EDTA-2K) within 30 min before dosing (0 h) and at 1, 2, 3, 4, 6, 8, 10, 12, 24, 48, 72, 96, 120, 168, and 216 h after almonertinib administration. Blood samples were centrifuged at 4 °C at 2000 rpm for 10 min within 60 min of blood collection. Plasma samples were stored at approximately −70 °C until analysis. Plasma concentrations of almonertinib and HAS-719 were determined using an API 5500 triple quadrupole mass spectrometer (AB Sciex, Concord, Ontario, Canada) coupled with an LC-30AD high-performance liquid chromatography system (Shimadzu, Kyoto, Japan). Data acquisition and processing were conducted using Analyst 1.6.3 software (AB Sciex, Concord, Ontario, Canada). Briefly, a protein-precipitation extraction procedure with acetonitrile was used to extract almonertinib and HAS-719 from human plasma samples. All analytes and the deuterium internal standard were separated on a BEH $C_{18}$ column (50 mm × 2.1 mm, Waters Corporation, Milford, MA, USA) using 5 mmol/L ammonium acetate with 0.1% formic acid (A) and acetonitrile (B) as the mobile phase at a flow of 0.55 mL/min with gradient elution: 20% B for 0.3 min; a stepwise linear increase to 90% B at 0.6 min; 0.6–1.4 min, 90% B; a stepwise linear decrease to 20% B at 1.6 min; 1.6–2.2 min, 20% B. Multiple reaction monitoring (*m/z* 526 → 411 for almonertinib, *m/z* 512 → 423 for HAS-719, and *m/z* 518 → 458 for d6-HAS-000719) was used in the positive electrospray ionization mode with an ion spray voltage of 5500 V and a source temperature of 550 °C. The nebulizer gas, heater gas and curtain gas were set to 50, 60, and 40 psi, respectively. The lower limits of

**Table 1.** Key inclusion and exclusion criteria for clinical studies.

| Inclusion criteria | Exclusion criteria |
|---|---|
| 1. Male and female subjects between ≥18 and ≤40 years of age, with a body mass index (BMI) between ≥19.0 and ≤28.0 kg/m$^2$ at screening;<br>2. Subjects in good health without heart, liver, kidney, digestive tract, nervous system, respiratory system, mental disorders or metabolic abnormalities history;<br>3. Written informed consent;<br>4. Taken effective contraceptive measures within 14 days prior to screening, no pregnancy plans during the study period and within; 6 months after the study. | 1. History of dysphagia or any gastrointestinal disease affecting drug absorption;<br>2. Use of prescription drugs within 14 days before administration of the study drug;<br>3. Use of over-the-counter medicine, Chinese herbal medicine or health supplement within 7 days administration of the study drug;<br>4. Use of drugs that inhibit or induce liver metabolism within 30 days prior to administration of the study drug;<br>5. History of surgery or participation in other drug clinical trials within 3 months prior to administration of the study drug;<br>6. Infection with human immunodeficiency virus (HIV), hepatitis B, hepatitis C, or syphilis virus;<br>7. Drug or alcohol abuse, smoker who consumes more than 5 cigarettes per day;<br>8. Pregnant or breast feeding or woman of positive pregnancy test result;<br>9. History of drug abuse or allergies. |

quantification of almonertinib/HAS-719 and their linear calibration range were 0.500/0.500 ng/mL and 0.500–500/0.500–500 ng/mL, respectively. Precision and accuracy of the method were evaluated by analyzing quality control (QC) samples at the LLOQ (0.500/0.500 ng/mL), low QC (1.50/1.50 ng/mL), medium QC (50.0/50.0 ng/mL) and high QC (400/400 ng/mL). In all QC concentrations, the coefficient of variation (CV) and accuracy were ≤10.0% and 91.7%–100% for almonertinib, ≤5.6% and 91.5%–100.8% for HAS-719, respectively.

In vitro studies

*Metabolism of HAS-719*. Human recombinant CYP enzymes (CYP1A2, CYP2A6, CYP2B6, CYP2C8, CYP2C9, CYP2C19, CYP2D6, CYP2E1, CYP3A4, and CYP3A5) were incubated with 3 μM HAS-719. The incubation mixtures (100 μL) consisted of phosphate buffer (100 mM, pH 7.4) with 3.2 mM $MgCl_2$, CYP enzymes (50 pmol/mL), and NADPH (1 mM). After 60-min incubation at 37 °C, ice-cold acetonitrile (100 μL) was added to each incubation mixture to stop the reaction.

To determine the contribution of CYP3A to the metabolism of HAS-719, the selective CYP3A inhibitor ketoconazole (KET, 2 μM) or the broad-spectrum inhibitor 1-aminobenzotriazole (ABT, 1 mM) was incubated with human liver microsomes (HLMs, 0.5 mg protein/mL) (100 μL) containing 3 μM HAS-719 and 1 mM NADPH. Ice-cold acetonitrile (100 μL) was added to stop the reaction at 0, 5, 15, 30, and 60 min after incubation at 37 °C.

*P-gp transport studies*. MDCKII-MDR1 cells were cultured in DMEM supplemented with 10% FBS, 2 mM *L*-glutamine, 100 U/mL penicillin G, 100 μg/mL streptomycin, and 1% minimum essential medium nonessential amino acids at 37 °C in a humidified 5% $CO_2$ atmosphere. The cells were seeded at a density of $2 \times 10^5$ cells/cm$^2$ on a polycarbonate membrane filter membrane on transwell inserts (Millipore, Billerica, MA, USA) and grown as monolayers for 5 days, and the medium was replaced every other day.

Before starting the experiment, cells were washed twice with prewarmed Hank's balanced salt solution (HBSS) and incubated with or without GF120918 (10 μM, P-gp inhibitor) for 30 min. The transport assay was initiated by addition of HAS-719 (10 μM) or almonertinib (10 μM) to the donor side (either the apical or basolateral chamber), and the positive inhibitors to both chambers. The cells were incubated for 90 min at 37 °C, at which time aliquots (200 μL) were collected from the receiver compartments for analysis. The samples were stored at −20 °C before liquid chromatography with tandem mass spectrometry (LC-MS/MS) analysis. Digoxin (10 μM, P-gp-positive substrate) was used for validation of the above efflux system.

Apparent permeability coefficients ($P_{app}$) were calculated using the equation $P_{app} = C_{receiver} \times V_{receiver}/(C_0 \times T \times S)$, where $C_{receiver}$ is the concentration of the test compound on the receiver side (nM), $V_{receiver}$ is the volume of the receiver well (mL), $S$ is the surface area of the cell monolayer (0.33 cm$^2$ in a 24-well plate), $C_0$ is the initial concentration in the donor well and $T$ is the transport time (min). The efflux ratio (ER) was defined as the B-to-A $P_{app}$ divided by the A-to-B $P_{app}$. The unpaired Student's *t*-test was used for statistical comparisons between two groups using GraphPad Prism (version 8.01; GraphPad Software Inc., La Jolla, CA, USA).

Animal studies

*Animals*. Beagle dogs were from shanghai Jambo Biological Technology Co. Ltd. Five 12-month-old healthy male Beagle dogs, weighing 10 to 15 kg were used. Each dog was housed in an individual cage and received water *ad libitum* and dry food twice a day. All procedures involving animals were in accordance with the *Guide for the Care and Use of Laboratory Animals* of the Shanghai Institute of Materia Medica, Chinese Academy of Sciences and approved by the Institutional Animal Care and Use Committee.

*Study design*. Almonertinib was dissolved in normal saline containing 5% dimethyl sulfoxide. Dogs were fasted for 12 h with free access to water before the experiments. On the first day, all dogs received a single oral gavage dose of 1 mg/kg almonertinib. Blood samples (1 mL) were collected from the jugular vein before the dose (0 h) and 0.25, 0.5, 1, 2, 4, 6, 8, 10, 24, and 48 h post-dosing. Feces was collected every 24 h until 96 h after dose. Blood samples were placed in EDTA-2K-containing tubes and immediately centrifuged at $3000 \times g$ for 10 min at 4 °C. After a 3-day wash-out period, all dogs received an oral dose of 100 mg rifampicin capsule once daily for 7 consecutive days (from day 6 to day 12). On day 13, dogs were fasted for 12 h with free access to water before the experiments and received a single oral gavage dose of 1 mg/kg almonertinib 30 min after rifampicin administration. Blood was sampled up to 48 h after treatment. Feces were collected every 24 h for 4 days after almonertinib administration. The fecal samples were homogenized with acetonitrile-water (1:1, *v/v*) at a ratio of 1:5 (*w/v*). All samples were stored at −70 °C until analysis.

*Sample analyses*. Almonertinib and HAS-719 content in dog plasma and fecal samples were analyzed as described in *"Clinical studies"*. Semi-quantitative analysis of other metabolites in fecal homogenate was performed (Supplementary data). The cumulative recovery of the metabolites was expressed by the peak area ratio of the analyte to the internal standard × volume of fecal homogenate/dose.

Metabolite profiling and identification

*Sample preparation*. Human plasma samples were segregated by sampling collection time (0, 2, 4, 10 and 24 h), and equal volumes (20 μL) from each subject (control group, rifampicin group or itraconazole group) were pooled. Then 3000 μL of acetonitrile was added to 600 μL of the pooled plasma sample. Two grand pools of fecal homogenate samples (0 h, 0–24 h) from control group and rifampicin group were separately prepared by combining volumes that are proportional to the total volume at each fecal homogenate from all dogs. The human plasma or dog fecal homogenate mixture was vortexed for 1 min, followed by centrifugation at $12{,}000 \times g$ for 5 min. The supernatant was transferred to a clean glass tube and evaporated to dryness under nitrogen at 40 °C. The reconstituted solution consisted of 200 μL of acetonitrile-water (1: 9, *v/v*).

*Instruments and data analysis*. Chromatographic separation for metabolite profiling was achieved using an Acquity UPLC system (Waters, Milford, MA, USA) on an Acquity UPLC HSS T3 column (1.8 μm, 2.1 mm × 100 mm; Waters). The mobile phase was a mixture of 0.1% formic acid in 5 mmol/L ammonium acetate (A) and acetonitrile (B). The gradient elution started from 10% B, increased linearly to 50% B over 8 min, increased linearly to 99% B over the next 0.5 min, was maintained at 99% B for 1.5 min, and finally decreased to 10% B to re-equilibrate the column. The column temperature was set at 40 °C, and the flow rate was 0.35 mL/min. The elute was monitored by UV detection at 270 nm. The MS detection was conducted by the Triple TOF 5600+ high-resolution mass spectrometer, equipped with a DuoSpray ionization source (AB Sciex, Concord, Ontario, Canada) operated in positive ion electrospray mode. Data were acquired using an ion spray voltage of 5500 V. Nitrogen settings for the curtain plate (CUR), the nebulizer (GS1) and the heater (GS2) were 40, 50, and 50, respectively. The interface heater temperature was maintained at 500 °C with decluster potential set at 80 V. Collision energies of 10 and 50 eV were used for time of flight mass spectrometry (TOF MS) and product ion scans, respectively, and a collision energy spread of 20 eV was used in the MS/MS experiment. All mass spectra were collected using the profile mode with the start and end mass set, respectively, at *m/z*

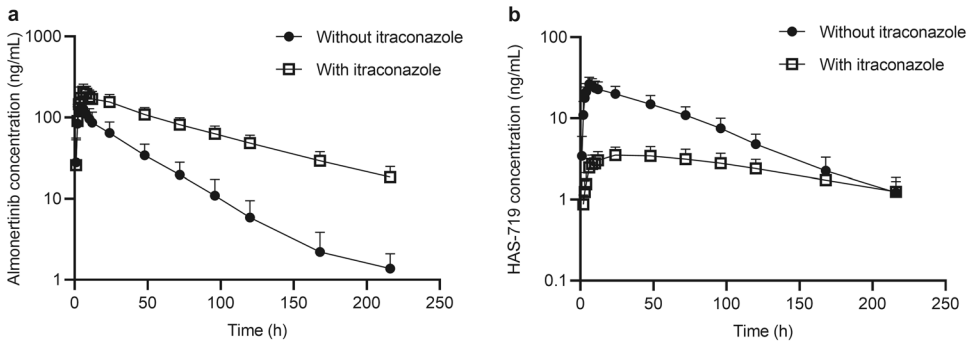


**Fig. 2 Mean plasma concentration–time profiles of almonertinib and HAS-719 following administration of 110 mg almonertinib with or without itraconazole in healthy adults. a** Almonertinib; **b** HAS-719; data shown as Mean ± SD ($n = 32$).

**Table 2.** Pharmacokinetics of almonertinib and HAS-719 following oral administration of 110 mg almonertinib without or with itraconazole (200 mg, bid).

| Analyte | Parameters | Summary statistic | Almonertinib 110 mg | | Ratio (%) | 90% CI of Ratio |
|---|---|---|---|---|---|---|
| | | | Alone ($n = 32$) | + Itraconazole ($n = 32$) | | |
| Almonertinib | $C_{max}$, ng/mL | Gmean (CV%) | 133 (36.3) | 208 (23.1) | 156 | 144.5–169.1 |
| | $AUC_{0-t}$, μg·h/mL | Gmean (CV%) | 4.42 (37.2) | 14.9 (22.4) | 338 | 312.2–365.8 |
| | $AUC_{0-\infty}$, μg·h/mL | Gmean (CV%) | 4.47 (37.3) | 16.7 (23.6) | 373 | 344.5–403.7 |
| | $T_{max}$, h | Median (range) | 4.00 (3.00–6.00) | 6.00 (4.00–12.00) | | |
| | $t_{1/2z}$, h | Mean (SD) | 29.7 (5.8) | 65.9 (9.4) | | |
| | CL/F, L/h | Mean (SD) | 26.4 (9.9) | 6.79 (1.67) | | |
| HAS-719 | $C_{max}$, ng/mL | Gmean (CV%) | 26.7 (19.9) | 3.52 (26.7) | 13.2 | 12.2–14.2 |
| | $AUC_{0-t}$, μg·h/mL | Gmean (CV%) | 1.80 (23.1) | 0.508 (29.0) | 28.2 | 25.8–30.9 |
| | $AUC_{0-\infty}$, μg·h/mL | Gmean (CV%) | 1.88 (24.0) | 0.693 (30.3) | 36.9 | 33.7–40.4 |
| | $T_{max}$, h | Median (range) | 6.00 (3.00–48.0) | 24.0 (24.0–96.0) | | |
| | $t_{1/2z}$, h | Mean (SD) | 45.1 (8.7) | 106 (23) | | |

80 and *m/z* 1000. The Q-TOF method consisted of a full scan TOF survey and four MS/MS product ion scans in information dependent acquisition (IDA) mode. Automatic calibrant delivery system (CDS) was programmed to deliver the reference solution through the APCI inlet of the DuoSpray ionization source. No additional internal lock mass was used. Data were acquired by Masslynx V4.1 (Waters Corporation, MA, USA) and Analyst®TF V1.6 software (AB Sciex, Concord, Ontario, Canada) and processed by PeakView® V1.2 and MetabolitePilot V1.5 software (AB Sciex, Concord, Ontario, Canada).

### Pharmacokinetic and statistical analyses

The pharmacokinetic parameters including the area under the plasma concentration–time curve from time of administration to the time of the last quantifiable concentration ($AUC_{0-t}$), the AUC from time zero of administration to infinity ($AUC_{0-\infty}$), apparent clearance (CL/F), and apparent terminal elimination half-life ($t_{1/2z}$) were calculated by noncompartmental analysis using WinNonlin 6.4 (Pharsight Corp, Mountain View, CA, USA). The maximal plasma concentration ($C_{max}$) and time to $C_{max}$ ($T_{max}$) were observed values. Statistical analyses were performed using the log-transformed data of $C_{max}$ and AUCs. The magnitude of the DDI was evaluated by computing the ratio of the geometric means (GMRs) of the drug in combination versus alone and the corresponding 90% confidence intervals (CIs) based on the log-transformed data. If 90% CIs of the ratio of GMRs of the PK parameters were within 80%–125%, then this was considered as the absence of a drug interaction.

## RESULTS

### Clinical studies

*Effect of itraconazole on the PK of almonertinib and HAS-719 (study 1).* The mean plasma concentration–time profile for almonertinib administered alone or in combination with itraconazole (200 mg, bid) are shown in Fig. 2 and the corresponding PK parameters are listed in Table 2.

The plasma concentrations of almonertinib were elevated at all time points after administration of itraconazole compared to almonertinib alone. The median $T_{max}$ of almonertinib was observed at 4 and 6 h with or without itraconazole, respectively. The $C_{max}$ and $AUC_{0-t}$ values of almonertinib were increased by 56.3% and 2.38-fold when almonertinib was co-administered with itraconazole. Consistent with a longer $t_{1/2z}$ in the presence of itraconazole (65.9 h), the mean clearance (CL/F) of almonertinib was decreased by ~74.3% relative to almonertinib alone. The GMRs and their associated 90% CIs for the comparison of almonertinib with and without itraconazole did not fall within the 80%–125% boundary, suggesting that itraconazole contributed to increase in plasma concentrations of almonertinib and decrease in its clearance.

As expected, concomtinant administration of almonertinib with itraconazole significantly decreased the $C_{max}$ and $AUC_{0-t}$ values of HAS-719 by 86.8% and 71.8%, respectively, which suggested that itraconazole inhibited the production of HAS-719 in vivo.

*Effect of rifampicin on the PK of almonertinib and HAS-719 (study 2).* After administration of almonertinib either alone or

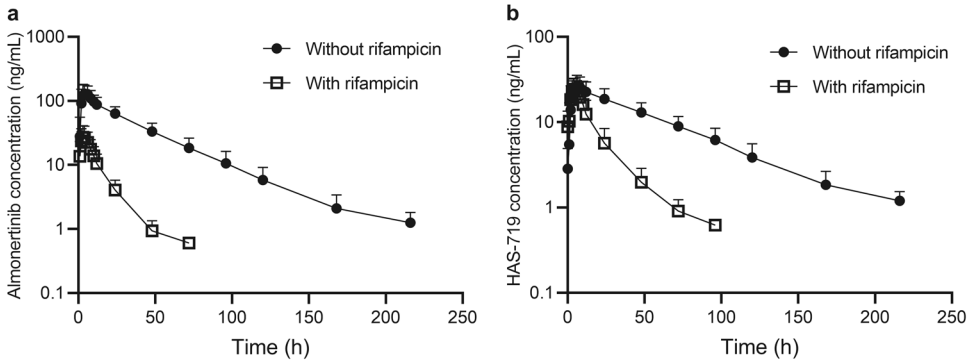


**Fig. 3 Mean plasma concentration–time profiles of almonertinib and HAS-719 following administration of 110 mg almonertinib with or without rifampicin in healthy adults. a** almonertinib; **b** HAS-719; data shown as Mean ± SD ($n = 32$).

**Table 3.** Pharmacokinetics of almonertinib and HAS-719 following oral administration of 110 mg almonertinib without or with rifampicin (600 mg, qd).

| Analyte | Parameters | Summary statistic | Almonertinib 110 mg | | Ratio (%) | 90% CI of Ratio |
|---|---|---|---|---|---|---|
| | | | Alone ($n = 32$) | + Rifampicin ($n = 32$) | | |
| Almonertinib | $C_{max}$, ng/mL | Gmean (CV%) | 135 (36.1) | 28.1 (44.1) | 20.7 | 18.6–23.1 |
| | $AUC_{0-t}$, μg·h/mL | Gmean (CV%) | 4.46 (31.9) | 0.328 (42.6) | 7.36 | 6.63–8.18 |
| | $AUC_{0-\infty}$, μg·h/mL | Gmean (CV%) | 4.51 (31.8) | 0.350 (39.8) | 7.75 | 7.02–8.56 |
| | $T_{max}$, h | Median (range) | 4.00 (2.00–10.0) | 3.00 (1.00–6.00) | | |
| | $t_{1/2z}$, h | Mean (SD) | 29.4 (5.9) | 9.15 (1.75) | | |
| | CL/F, L/h | Mean (SD) | 25.4 (7.3) | 335 (122) | | |
| HAS-719 | $C_{max}$, ng/mL | Gmean (CV%) | 27.1 (30.1) | 24.5 (32.3) | 90.5 | 82.8–98.9 |
| | $AUC_{0-t}$, μg·h/mL | Gmean (CV%) | 1.71 (24.8) | 0.469 (28.8) | 27.5 | 25.3–29.9 |
| | $AUC_{0-\infty}$, μg·h/mL | Gmean (CV%) | 1.78 (23.8) | 0.490 (27.6) | 27.4 | 25.3–29.7 |
| | $T_{max}$, h | Median (range) | 6.00 (3.00–12.0) | 4.00 (4.00–8.00) | | |
| | $t_{1/2z}$, h | Mean (SD) | 44.0 (8.7) | 16.2 (3.9) | | |

in combination with rifampicin, mean plasma concentration–time profiles and PK parameters were measured (Fig. 3 and Table 3).

Rifampicin significantly reduced the plasma concentrations of almonertinib and shortened the $T_{max}$ (4 vs. 3 h). When almonertinib was co-administered with rifampicin, the $C_{max}$ and $AUC_{0-t}$ values of almonertinib were decreased by 79.3% and 92.6% and the CL/F of almonertinib was 12-fold higher compared with the administration of almonertinib alone. Furthermore, the mean $t_{1/2z}$ for almonertinib decreased from 29.4 h to 9.15 h. The 90% CI for GMRs (with vs. without rifampicin) of $C_{max}$ and $AUC_{0-t}$ of almonertinib did not fall within the 80%–125% boundary, suggesting that rifampicin affected the pharmacokinetics of almonertinib by inducing CYP3A. Combined with the decrease in $t_{1/2z}$, the results suggested that rifampicin significantly increased the plasma clearance of almonertinib.

It was interesting to note that the $C_{max}$ value of the active metabolite HAS-719 didn't change significantly with or without rifampicin. Moreover, the $AUC_{0-t}$ value of HAS-719 was reduced by 72.6%. It could be observed from the mean plasma concentration–time profiles of HAS-719 that the elimination rate of HAS-719 was increased in the presence of rifampicin.

### Metabolism of HAS-719 is mediated by CYP enzymes

In order to explore whether HAS-719 was further metabolized by CYPs, human recombinant CYP enzymes and HLMs were used to determine the enzyme phenotypes mediating the oxidative metabolism of HAS-719. HAS-719 was almost completely metabolized in the CYP3A4 incubation mixtures while not significantly changed in the other incubation mixtures (Fig. 4a). In the presence of the CYP3A inhibitor ketoconazole, the elimination rate of HAS-719 in human liver microsomes was significantly reduced, which was similar to that in the presence of ABT (CYP450 inhibitor) (Fig. 4b).

### Transport of almonertinib and HAS-719 across MDCKII-MDR1 cell monolayers

The changes in CL/F of almonertinib and HAS-719 didn't rule out the contribution of excretion. Both CYP3A and P-gp were regulated by the nuclear receptor PXR, which could be induced by rifampicin [12, 13]. Therefore, it seemed necessary to investigate whether almonertinib and HAS-719 were substrates of P-gp in order to assess the P-gp role in the pharmacokinetic interaction of rifampicin and almonertinib. The ERs of almonertinib and HAS-719 in MDCKII-MDR1 cells were 6.47 and 25.7, respectively, while in the presence of the potent inhibitor GF120918, the ERs were decreased to 0.793 and 1.65 (Table 4). Therefore, it could be concluded that both almonertinib and HAS-719 were the substrates of P-gp.

### Effect of rifampicin on the PK profile and excretion of almonertinib in beagle dogs

The in vitro study suggested that the production of HAS-719 in dogs was also mainly catalyzed by CYP3A, similar to that in humans (Supplementary Fig S2). To investigate the mechanisms underlying the AUC decrease of the metabolite HAS-719 in the presence of rifampicin, we conducted PK and excretion studies in

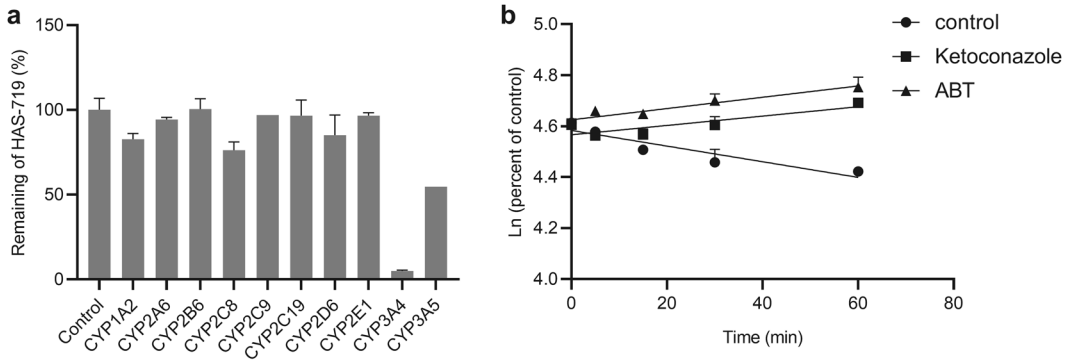


**Fig. 4 Metabolism of HAS-719 in vitro. a** recombinant human CYP enzymes; **b** human liver microsomes.

**Table 4.** Transport of almonertinib and HAS-719 across MDCKII-MDR1 cell monolayers.

| Substrates | $P_{app,a\rightarrow b}$ ($\times 10^{-6}$ cm/s) | $P_{app,b\rightarrow a}$ ($\times 10^{-6}$ cm/s) | ER |
|---|---|---|---|
| Almonertinib | 0.172 ± 0.026 | 1.11 ± 0.16 | 6.47 |
| Almonertinib + GF120918 | 0.635 ± 0.233* | 0.503 ± 0.170* | 0.793 |
| HAS-719 | 0.262 ± 0.119 | 6.74 ± 0.43 | 25.7 |
| HAS-719 + GF120918 | 0.327 ± 0.128 | 0.540 ± 0.095*** | 1.65 |
| Digoxin | 0.363 ± 0.041 | 8.90 ± 1.01 | 24.5 |
| Digoxin + GF120918 | 1.00 ± 0.13** | 3.70 ± 0.10** | 3.69 |

Data are expressed as mean ± SD ($n = 3$). *$P < 0.05$; **$P < 0.01$; *** $P < 0.001$. compared with the control group.

**Table 5.** Pharmacokinetics of almonertinib in beagle dogs (1 mg/kg, *p.o.*) with or without rifampicin.

| Analyte | Parameters | Alone | + Rifampicin |
|---|---|---|---|
| Almonertinib | $C_{max}$, ng/mL | 129 ± 20 | 91.5 ± 14.2** |
| | $AUC_{0-t}$, ng·h/mL | 934 ± 194 | 466 ± 80** |
| | $AUC_{0-\infty}$, ng·h/mL | 938 ± 196 | 476 ± 80** |
| | $T_{max}$, h | 2.00 (2.00)[a] | 2.00 (1.00–2.00)[a] |
| | $T_{1/2}$, h | 6.44 ± 0.47 | 3.15 ± 0.89 |
| HAS-719 | $C_{max}$, ng/mL | 34.2 ± 5.2 | 38.5 ± 3.6 |
| | $AUC_{0-t}$, ng·h/mL | 332 ± 29 | 315 ± 49 |
| | $AUC_{0-\infty}$, ng·h/mL | 334 ± 30 | 316 ± 50 |
| | $T_{max}$, h | 2.00 (2.00)[a] | 2.00 (2.00)[a] |
| | $T_{1/2}$, h | 6.55 ± 0.61 | 5.13 ± 0.77 |

Data are expressed as mean ± SD ($n = 5$). **$P < 0.001$ vs. the control.
[a]Median (range).

beagle dogs. When almonertinib was co-administered with rifampicin, the plasma exposure and $t_{1/2}$ of almonertinib were reduced by 50%, while the PK profile of the metabolite HAS-719 was unchanged (Table 5). Preclinical studies had shown that almonertinib and its metabolites were mainly excreted through feces, and the urine excretion was negligible (Hansoh unpublished data). Therefore, only the fecal recovery of almonertinib and HAS-719 in dogs was investigated. In the rifampicin group, the fecal recovery of almonertinib and HAS-719 decreased from 1.01% to 0.214% and 2.81% to 0.822%, respectively, indicating that rifampicin induced the metabolism of HAS-719 rather than accelerating its excretion due to the induction of P-gp (Fig. 5).

Metabolic profile of almonertinib in human plasma and dog feces
The metabolic profiles of almonertinib in human plasma and dog feces are shown in Supplementary Fig S3. In human plasma, a total of 8 metabolites were detected, and the principle metabolic pathways were identified as *N*-dealkylation, oxidation and glucuronide conjugation (Fig. 6). Among them, *N*-dealkylated ($-C_4H_9N$) and *N*-demethylated metabolite M1, *N*-dealkylated ($-C_4H_9N$) metabolite M2 and *N*-dealkylated ($-C_{15}H_{21}N_3O_2$) metabolite M30 could be generated from the further metabolism of HAS-719 catalyzed by CYP3A4 (data not shown), and their plasma exposures were increased in the rifampicin group or decreased in the itraconazole group (Fig. 7b1–b4). In addition to M1, M2, and M30 as the downstream metabolites of HAS-719, *N*-demethylated and oxidized metabolites M6-1/M6-2, *N*-desdimethylated metabolites M4-1/M4-2, oxidative and deaminated metabolite M33, *N*-dealkylated ($-C_4H_9N$) and oxidative metabolite M34-1/M34-2, *N*-desmethylated and N-descyclopropylated metabolite M35, and oxidized and sulfate conjugated metabolite M37 were also detected in dog feces (Fig. 6). When co-administered with rifampicin, the fecal recovery of M1, M4-1, M4-2, and M33 were significantly increased compared to the almonertinib group (Fig. 7a1–a4).

## DISCUSSION

In vitro metabolism studies have shown that almonertinib was primarily metabolized by CYP3A. NSCLC patients may have co-morbidities and need multidrug therapy, which may include CYP3A inhibitors or inducers. When patients are administered almonertinib with other drugs as the perpetrators of CYP3A, PK profile of almonertinib may be altered, and this could affect the efficacy and/or safety of almonertinib. The present two-arm study examined the effects of itraconazole (a potent CYP3A inhibitor) or rifampicin (a potent CYP3A inducer) on the PK of almonertinib in healthy subjects. As HAS-719 was previously identified as the main active metabolite in human plasma whose plasma exposure was about 40% of the parent drug, we also investigated the pharmacokinetics of HAS-719 in the present study.

Clinical trials have shown that itraconazole and rifampicin have a significant impact on the PK of almonertinib and its metabolite HAS-719. Itraconazole and rifampicin are modulators of both CYP3A and P-gp. The importance of enzyme-transporter interplay has been extensively investigated, especially CYP3A and P-gp, because they shared overlapping substrates and common nuclear receptors [14, 15]. For example, case reports have shown that ranolazine inhibition of P-gp and CYP3A is linked to increased sirolimus [16] or simvastatin [17] exposure in humans. Another in vitro study revealed that when the activity of P-gp was inhibited, the metabolism of sirolimus via CYP3A4 was affected [18]. Since both almonertinib and HAS-719 are

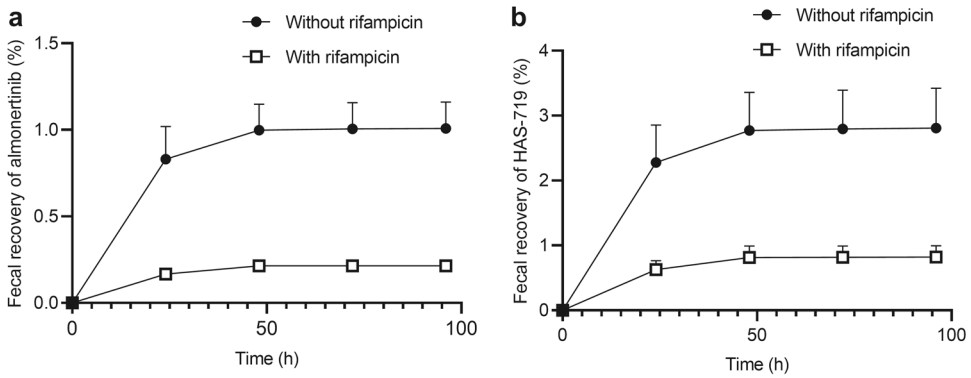


**Fig. 5 Fecal recovery–time profiles of almonertinib and HAS-719 following administration of 1 mg/kg almonertinib with or without rifampicin in beagle dogs. a** Almonertinib; **b** HAS-719; data shown as Mean ± SD ($n = 5$).

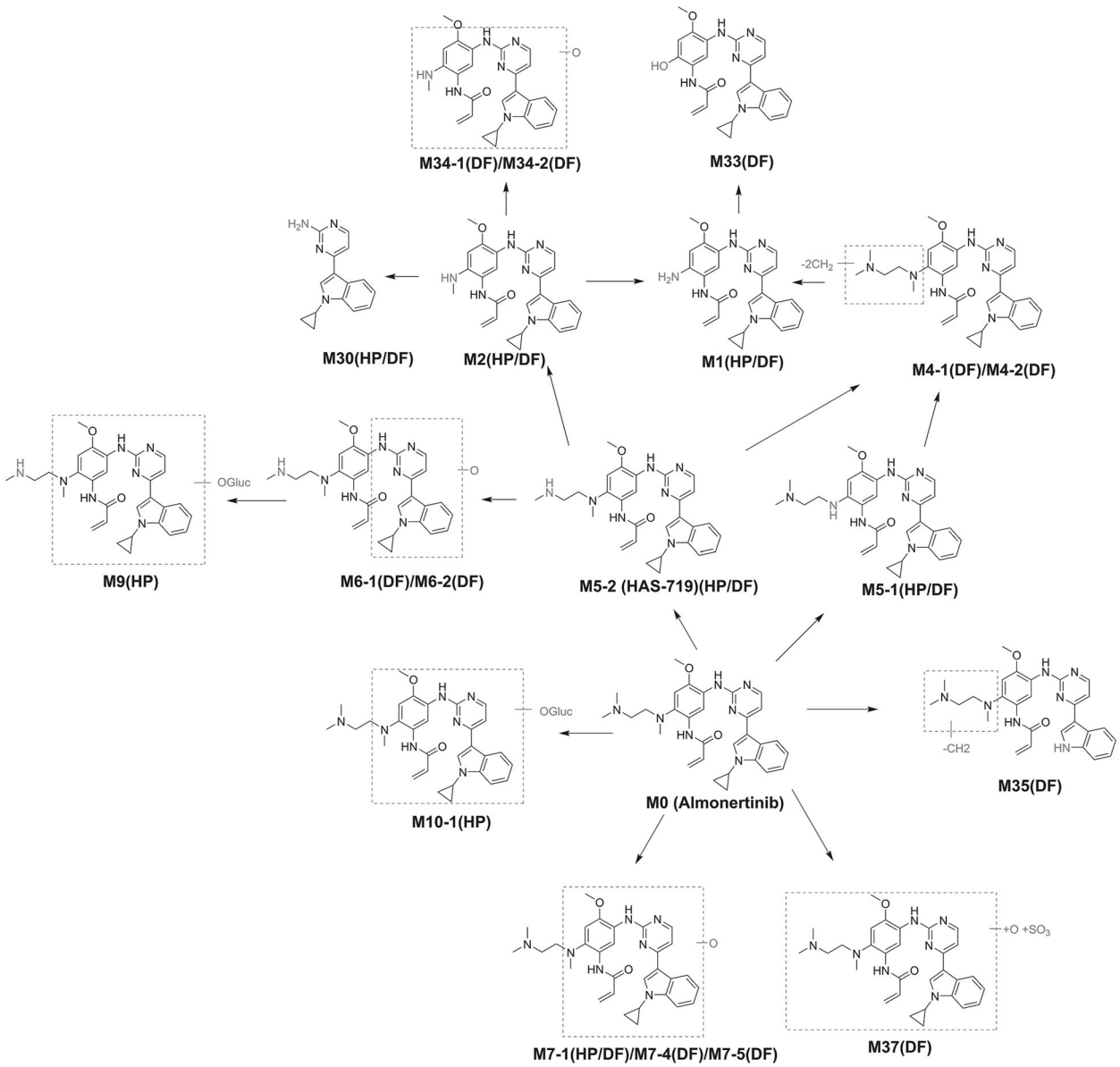


**Fig. 6** Metabolic pathways of almonertinib in human plasma (HP) and dog feces (DF).

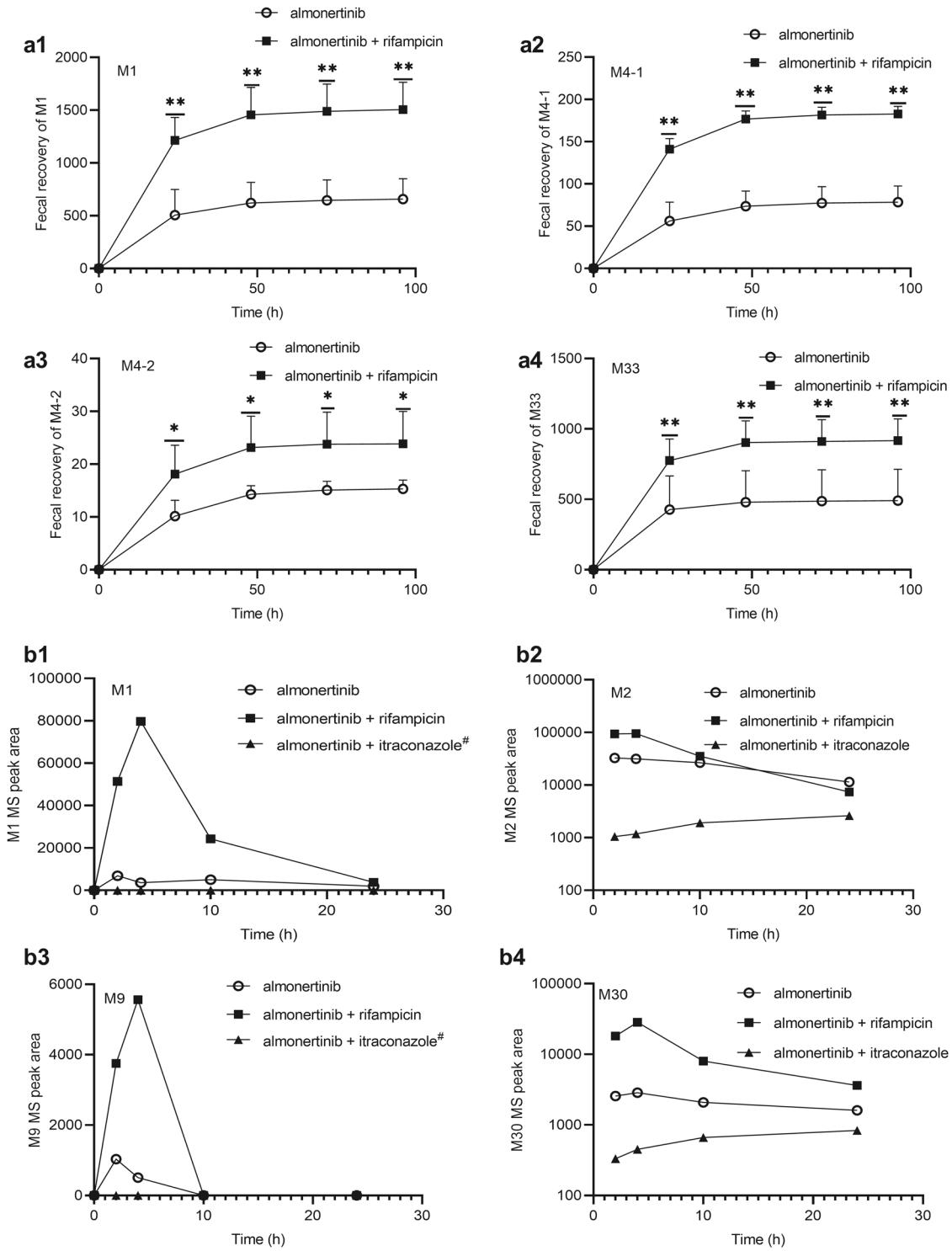


**Fig. 7 Mass peak area-time profiles of metabolites in dog feces and human plasma with or without rifampicin/itraconazole. a1** M1 in dog feces; **a2** M4-1 in dog feces; **a3** M4-2 in dog feces; **a4** M33 in dog feces; **b1** M1 in human plasma; **b2** M2 in human plasma; **b3** M9 in human plasma; **b4** M30 in human plasma; fecal recovery is expressed as the area ratio of analyte to internal standard × fecal homogenate volume/dose; #: M1 and M9 were not determined in the itraconazole group; *$P < 0.05$; **$P < 0.01$).

substrates of CYP3A and P-gp, the role of P-gp should be addressed.

Theoretically, the inhibition of P-gp will increase the plasma exposures of both almonertinib and HAS-719. However, in our study determining the interactions of itraconazole and almonertinib, there was a decrease of the $C_{max}$ and $AUC_{0-t}$ values of HAS-719 and an increase of the $C_{max}$ and $AUC_{0-t}$ values for almonertinib. This resulted in a significant reduction of the plasma exposure ratio of the metabolite to the parent drug, suggesting that itraconazole mainly affected the metabolism of almonertinib rather than excretion. Even though HAS-719 is CYP3A4 substrate, the formation of HAS-719 was preferentially inhibited, as a result, the inhibition of itraconazole on the further metabolism of HAS-719 had no effect on plasma exposure.

In comparison, rifampicin co-administration with almonertinib decreased the $C_{max}$ and $AUC_{0-t}$ of almonertinib, and also decreased the $AUC_{0-t}$ of HAS-719. The upregulation of both CYP3A4 and P-gp could lead to the reduction of the plasma exposure of HAS-719, and the roles of CYP3A4 and P-gp in the PK alteration of HAS-719 were still unknown. To better understand this relationship, PK and excretion studies were conducted in beagle dogs because the in vivo and in vitro metabolic studies showed that almonertinib exhibited similar metabolic pathways and enzymes in dogs and humans. The downstream metabolites of HAS-719 measured in dog feces were significantly increased when co-administered with rifampicin. In particular, a significant decrease in the fecal recovery of almonertinib and HAS-719 was an indication that the metabolism of almonertinib and HAS-719 was modified by rifampicin, rather than increased excretion. This finding for HAS-719 and its downstream metabolites was consistent with that from human plasma studies. In addition, the pronounced increase of $C_{max}$ ratio for the metabolite HAS-719 to the parent drug (from 20.1% to 87.2%) as well as $AUC_{0-t}$ ratio (from 38.3% to 143%) in humans provided further evidence supporting the idea that rifampicin induced the metabolism rather than excretion of almonertinib.

Rifampicin induced almonertinib to a different extent in humans and dogs, which may be attributed to two factors. On the one hand, there may be species differences in the induction of CYP3A by rifampicin. It has been reported that under the same concentration of rifampicin, the fold increase of CYP3A mRNA in dog liver was significantly lower than that in human liver [19]. On the other hand, there may be differences in experimental design. In the present clinical study, after co-administration of rifampicin with almonertinib, rifampicin continued to be administered once daily until the end of blood collection. The plasma concentration of rifampicin was maintained at a steady level during the whole sampling period. In dog study, after rifampicin was administered together with almonertinib, rifampicin was discontinued. The plasma concentration of rifampicin in dogs decreases gradually during the whole sampling period.

In conclusion, a detailed understanding of the PK drug–drug interaction potential of almonertinib was conducted in the present study. Both itraconazole and rifampicin had a significant effect on the in vivo exposure of almonertinib in humans. Almonertinib was demonstrated to be a moderately sensitive substrate of CYP3A in vivo. Based upon our findings, we hypothesize that special attention should be paid to the interaction between drugs or food that affects the activity of CYP3A when almonertinib is used clinically. Moreover, it is not recommended to use almonertinib in combination with CYP3A inducers.

## ACKNOWLEDGEMENTS

This work was supported by the National Natural Science Foundation of China (Grant 82073924). We thank clinical staff of Ji-nan Central Hospital for their participating in the discussion of the clinical protocol, and being responsible for the management of the subjects and the collection of plasma samples. We are grateful for the contributions of the study sponsor, Hansoh Pharmaceutical Group Co. Ltd.

## AUTHOR CONTRIBUTIONS

LL and XYC participated in research design: LL, ZTG, NJX, HX, LY and WL conducted experiments: LL and XYC wrote the manuscript.

## ADDITIONAL INFORMATION

**Supplementary information** The online version contains supplementary material available at https://doi.org/10.1038/s41401-021-00710-8.

**Competing interests:** The authors declare no competing interests.

## REFERENCES

1. Sigismund S, Avanzato D, Lanzetti L. Emerging functions of the EGFR in cancer. Mol Oncol. 2018;12:3–20.
2. Janne PA, Yang JC, Kim DW, Planchard D, Ohe Y, Ramalingam SS, et al. AZD9291 in EGFR inhibitor-resistant non-small-cell lung cancer. N Engl J Med. 2015;372:1689–99.
3. Roskoski R Jr. Small molecule inhibitors targeting the EGFR/ErbB family of protein-tyrosine kinases in human cancers. Pharmacol Res. 2019;139:395–411.
4. Pao W, Chmielecki J. Rational, biologically based treatment of EGFR-mutant non-small-cell lung cancer. Nat Rev Cancer. 2010;10:760–74.
5. Yun CH, Mengwasser KE, Toms AV, Woo MS, Greulich H, Wong KK, et al. The T790M mutation in EGFR kinase causes drug resistance by increasing the affinity for ATP. Proc Natl Acad Sci U S A. 2008;105:2070–5.
6. Jackman D, Pao W, Riely GJ, Engelman JA, Kris MG, Janne PA, et al. Clinical definition of acquired resistance to epidermal growth factor receptor tyrosine kinase inhibitors in non-small-cell lung cancer. J Clin Oncol. 2010;28:357–60.
7. Yu HA, Arcila ME, Rekhtman N, Sima CS, Zakowski MF, Pao W, et al. Analysis of tumor specimens at the time of acquired resistance to EGFR-TKI therapy in 155 patients with EGFR-mutant lung cancers. Clin Cancer Res. 2013;19:2240–7.
8. Choo JR, Tan CS, Soo RA. Treatment of EGFR T790M-positive non-small cell lung cancer. Target Oncol. 2018;13:141–56.
9. Han W, Du Y. Recent development of the second and third generation irreversible epidermal growth factor receptor inhibitors. Chem Biodivers. 2017;14:201600372.
10. Jiang T, Luo Y, Wang B. Almonertinib-induced interstitial lung disease: a case report. Medicine (Baltimore). 2021;100:e24393.
11. Yang JC, Camidge DR, Yang CT, Zhou J, Guo R, Chiu CH, et al. Safety, efficacy, and pharmacokinetics of almonertinib (HS-10296) in pretreated patients with EGFR-mutated advanced NSCLC: a multicenter, open-label, phase 1 trial. J Thorac Oncol. 2020;15:1907–18.
12. Lutz JD, Kirby BJ, Wang L, Song Q, Ling J, Massetto B, et al. Cytochrome P450 3A induction predicts p-glycoprotein induction; part 1: establishing induction relationships using ascending dose rifampin. Clin Pharmacol Ther. 2018;104:1182–90.
13. Hanke N, Frechen S, Moj D, Britz H, Eissing T, Wendl T, et al. PBPK models for CYP3A4 and P-gp DDI prediction: a modeling network of rifampicin, itraconazole, clarithromycin, midazolam, alfentanil, and digoxin. CPT Pharmacomet Syst Pharmacol. 2018;7:647–59.
14. Benet LZ. The drug transporter-metabolism alliance: uncovering and defining the interplay. Mol Pharmacol. 2009;6:1631–43.
15. Benet LZ, Cummins CL, Wu CY. Transporter-enzyme interactions: implications for predicting drug-drug interactions from in vitro data. Curr Drug Metab. 2003;4:393–8.
16. Masters JC, Shah MM, Feist AA. Drug interaction between sirolimus and ranolazine in a kidney transplant patient. Case Rep Transpl. 2014;2014:548243.
17. Hylton AC, Ezekiel TO. Rhabdomyolysis in a patient receiving ranolazine and simvastatin. Am J Health Syst Pharm. 2010;67:1829–31.
18. Cummins CL, Jacobsen W, Christians U, Benet LZ. CYP3A4-transfected Caco-2 cells as a tool for understanding biochemical absorption barriers: studies with sirolimus and midazolam. J Pharmacol Exp Ther. 2004;308:143–55.
19. Chen J, Tran C, Xiao L, Palamanda J, Klapmuts T, Kumari P, et al. Co-induction of CYP3A12 and 3A26 in dog liver slices by xenobiotics: species difference between human and dog CYP3A induction. Drug Metab Lett. 2009;3:61–6.